Journal of Solid State Chemistry **153,** 330–335 (2000)
doi:10.1006/jssc.2000.8778, available online at http://www.idealibrary.com on IDEAL®

Crystal Structures and Magnetic Properties of Quaternary Manganese Sulfides, BaLn_2MnS_5 (Ln = La, Ce, and Pr)

Makoto Wakeshima and Yukio Hinatsu

Division of Chemistry, Graduate School of Science, Hokkaido University, Sapporo 060-0810, Japan

Received February 1, 2000; revised May 5, 2000; accepted May 18, 2000; published online July 7, 2000

The crystal structures and magnetic properties of quaternary manganese sulfides BaLn_2MnS_5 (Ln = La, Ce, and Pr) are reported. The quaternary manganese sulfides were synthesized by a solid state reaction and determined to have tetragonal structures with space group *I*4/*mcm* by the Rietveld method. Their EPR spectra show that the Mn ions are in the $^6S_{5/2}$ state. The magnetic susceptibilities and the specific heats were measured from 2 to 300 K. The results of the measurements for $BaLa_2MnS_5$, $BaCe_2MnS_5$, and $BaPr_2MnS_5$ exhibit the antiferromagnetic orderings for Mn^{2+} ions at 58.5, 62, and 64.5 K, respectively. For $BaCe_2MnS_5$ and $BaPr_2MnS_5$, the Ce and Pr ions are in the paramagnetic state down to 2 K. The specific heat for $BaCe_2MnS_5$ shows a Schottky anomaly at low temperatures.

Key Words: **manganese; sulfide; crystal structure; magnetic property; antiferromagnetic transition.**

INTRODUCTION

Many ternary and quaternary manganese sulfides have crystal structures containing manganese ions coordinated tetrahedrally to four sulfur ions. For example, $A_xMn_yS_z$ (A = alkali metal) compounds crystallize in structures which contain anionic building units Mn_yS_z formed by linkage of MnS_4 tetrahedra via their corners (1). A ternary manganese sulfide, Ba_2MnS_3, crystallizes in an orthorhombic structure and the MnS_4 tetrahedra form infinite linear chains through corner-sharing (2). In a quaternary manganese sulfide, Cu_2MnSnS_4, the MS_4 (M = Mn, Cu, Sn) tetrahedra share their corners and the Mn ions form a body-centered tetragonal lattice (3). For K_2MnSnS_4, corner-sharing MS_4 tetrahedra (M = Mn and Sn) form M_4S_{10} tetrameric clusters, and the tetrameric clusters and K ions crystallize in a monoclinic structure (4).

These ternary and quaternary manganese sulfides show interesting magnetic behavior and undergo magnetic orderings at low temperatures. The Ba_2MnS_3 exhibited a one-dimensional Heisenberg-type magnetic ordering which could be explained by a linear-chain model of MnS_4 tetrahedra (2). For Cu_2MnSnS_4, the antiferromagnetic structure was determined by neutron diffraction measurement, and the magnetization curve showed the presence of a spin flop phase below the Néel temperature (3, 5). Peculiar magnetic properties of K_2MnSnS_4 could be explained by a model containing no exchange interaction between M_4S_{10} clusters (4).

Recently, Masuda *et al.* reported the synthesis of a new quaternary manganese sulfide, $BaLa_2MnS_5$ (6). Its crystal structure was a tetragonal structure based on stacking of the $BaMnS_4$ layers and La_2S layers. In the $BaMnS_4$ layer, the MnS_4 tetrahedra are linked by the Ba ions. The electrical conductivity of $BaLa_2MnS_5$ was reported to be semiconductive (6).

In this study, we attempted to synthesize a series of BaLn_2MnS_5 (Ln = lanthanides). For Ln = La, Ce, and Pr, single phase compounds were successfully prepared and they are isostructural. We measured their magnetic susceptibilities, magnetization, specific heats, and electron paramagnetic resonance (EPR) spectra.

EXPERIMENTAL

Attempts were made to synthesize quaternary manganese sulfides, BaLn_2MnS_5 (Ln = La, Ce, Pr, Nd, Sm, and Eu), by a solid state reaction process. Barium sulfide (BaS), manganese monosulfide (MnS), and lanthanide sulfides (Ln_2S_3 (Ln = La, Ce, Pr, Nd, Sm, EuS) were used as starting materials. The stoichiometric mixtures were ground and put into a quartz tube, and the tube was evacuated and sealed. Then, the ampoule was heated at 1273 K for 3 days with regrinding at intervals.

The products were characterized by determination of their X-ray diffraction profiles, which were obtained using a Rigaku RINT2200 diffractometer with graphite-monochromated Cu $K\alpha$ radiation in the range $10 \leq 2\theta/^\circ \leq 120$ ($\Delta 2\theta = 0.02^\circ$). The crystal structures were refined by the Rietveld method (RIETAN-97 program (7)). A pseudo-Voigt profile function was used to describe the peak shape.

0022-4596/00 $35.00

The EPR spectrum was obtained at room temperature with a JEOL RE2X spectrometer at an X band frequency of ca. 9.4 GHz. The magnetic field was monitored with a proton NMR gaussmeter.

The temperature dependence of the magnetic susceptibilities was measured under both zero-field-cooled (ZFC) and field-cooled (FC) conditions in the temperature range between 2 and 300 K by using a SQUID magnetometer (Quantum Design, MPMS-5S). The ZFC susceptibility measurements were performed under an applied magnetic field of 0.1 T, after the sample was cooled from 300 to 2 K in a zero field. For FC susceptibility measurements, the sample was cooled in the presence of a field, 0.1 T. Detailed temperature dependence of the susceptibilities was measured in the neighbourhood of the magnetic transition temperatures. The field dependence of the magnetization was measured at 2 K by changing the magnetic field between -5 and 5 T.

The specific heat measurement was carried out using a relaxation technique supplied by the commercial specific heat measurement system (Quantum Design, PPMS) in the temperature range from 1.8 to 300 K. The sample in the form of pellet ($\sim$7 mg) was mounted on an alumina plate with apiezon for better thermal contact.

RESULTS AND DISCUSSION

Crystal Structures

The powder productions, $BaLa_2MnS_5$, $BaCe_2MnS_5$, and $BaPr_2MnS_5$ were brown, black, and dark orange in color, respectively. By the Rietveld method, their powder X-ray diffraction profiles were indexed on tetragonal cells with the space group $I4/mcm$, and their crystallographic parameters were refined. Three positional parameters reported by Masuda *et al.* (6) were used as the initial positional parameters. The lattice parameters were calculated by the least-squares method. In these compounds, barium, lanthanide, and manganese cations are located in 4*a* (0, 0, 1/4), 8*h* (x, $x + 1/2$, 0), and 4*b* (0, 1/2, 1/4) sites, respectively. Sulfur anions occupy two different sites, S(1) and S(2) in 4*c* (0, 0, 0) and 16*l* (x, $x + 1/2$, z), respectively. Attempts to synthesize compounds $BaNd_2MnS_5$, $BaSm_2MnS_5$, and $BaEu_2MnS_5$ resulted in the formation of mixtures containing unknown phases and/or the starting materials. Tables 1 and 2 list the refined lattice parameters, atomic positions, and bond lengths for $BaLa_2MnS_5$, $BaCeMnS_5$, and $BaPr_2MnS_5$. The final reliability factors are also listed in Table 1. The results for $BaLa_2MnS_5$ agree with the reported values (6).

The schematic structure of $BaLn_2MnS_5$ is illustrated in Fig. 1. The *Ln*–S layers and Ba–Mn–S layers, which are perpendicular to the *c*-axis, are stacked alternately. In the Ba–Mn–S layers, the Mn^{2+} ions are in a distorted tetrahedral coordination bonded to four sulfurs and these MnS_4 tetrahedra link via the Ba ions. Figure 2 shows the coordination of the *Ln* ion and the Ba ion. The coordination number of the Ba ion is 10; it has eight nearest-neighbor sulfur ions S(2) and two next-nearest-neighbor sulfur ions S(1). The *Ln* ion has eight sulfur neighbors and its coordination polyhedron is quite irregular as shown in Fig. 2.

For the $BaLn_2MnS_5$ compounds, both the *a* and *c* parameters increase with the ionic radius of the lanthanide ion and the variation of the *a* parameters is larger than that of the *c* parameters. The *a* parameters become larger in proportion to the *Ln*–S(1) bond lengths, because the S–*Ln*–S bond angles in the *Ln*–S layer scarcely change (141.2, 140.8, and 141.2° for $BaLa_2MnS_5$, $BaCe_2MnS_5$, and $BaPr_2MnS_5$, respectively). On the other hand, the effect of lanthanide ionic size on the *c* parameters is smaller than that on the

TABLE 1
Lattice Parameters and Atomic Positions of $BaLa_2MnS_5$

	Site	x	y	z	B/Å^2
$BaLa_2MnS_5$	Space group, $I4/mcm$, $a = 7.9974(1)$ Å, $c = 13.8536(2)$ Å				
($z = 4$)	$R_{wp} = 13.47\%$, $R_I/\% = 3.15$, $R_F = 1.90\%$				
Ba	4*a*	0	0	1/4	0.90
La	8*h*	0.1621(3)	0.6618	0	0.60
Mn	4*b*	0	1/2	1/4	0.54
S(1)	4*c*	0	0	0	0.91
S(2)	16*l*	0.1522(10)	0.6528	0.6355(6)	0.98
$BaCe_2MnS_5$	Space group, $I4/mcm$, $a = 7.9257(1)$ Å, $c = 13.8300(2)$ Å				
($z = 4$)	$R_{wp} = 13.28\%$, $R_I/\% = 3.26$, $R_F = 2.26\%$				
Ba	4*a*	0	0	1/4	0.73
Ce	8*h*	0.1610(3)	0.6610	0	0.26
Mn	4*b*	0	1/2	1/4	0.33
S(1)	4*c*	0	0	0	1.24
S(2)	16*l*	0.1516(9)	0.6516	0.6351(6)	0.90
$BaPr_2MnS_5$	Space group, $I4/mcm$, $a = 7.8868(1)$ Å, $c = 13.8004(2)$ Å				
($z = 4$)	$R_{wp} = 13.29\%$, $R_I/\% = 2.82$, $R_F = 1.84\%$				
Ba	4*a*	0	0	1/4	0.67
Pr	8*h*	0.1620(2)	0.6620	0	0.31
Mn	4*b*	0	1/2	1/4	0.26
S(1)	4*c*	0	0	0	0.46
S(2)	16*l*	0.1516(8)	0.6516	0.6330(5)	0.74

Note. $R_{wp} = [\sum w(|F(o)| - |F(c)|)^2/\sum w|F(o)|^2]^{1/2}$.
$R_I = \sum|I_k(o) - I_k(c)|/\sum I_k(o)$. $R_F = \sum|F_k(o) - F_k(c)|/\sum F_k(o)$.

TABLE 2
Bond Lengths of $BaLn_2MnS_5$ (*Ln* = La, Ce, Pr)

Bond Length r/Å	$BaLa_2MnS_5$	$BaCe_2MnS_5$	$BaPr_2MnS_5$
Ba–S(1) × 2	3.463	3.458	3.450
Ba–S(2) × 8	3.421	3.405	3.404
Ln–S(1) × 2	2.997	2.974	2.956
Ln–S(2) × 2	2.818	2.811	2.773
Ln–S(2) × 4	3.139	3.104	3.081
Mn–S(2) × 4	2.343	2.327	2.338

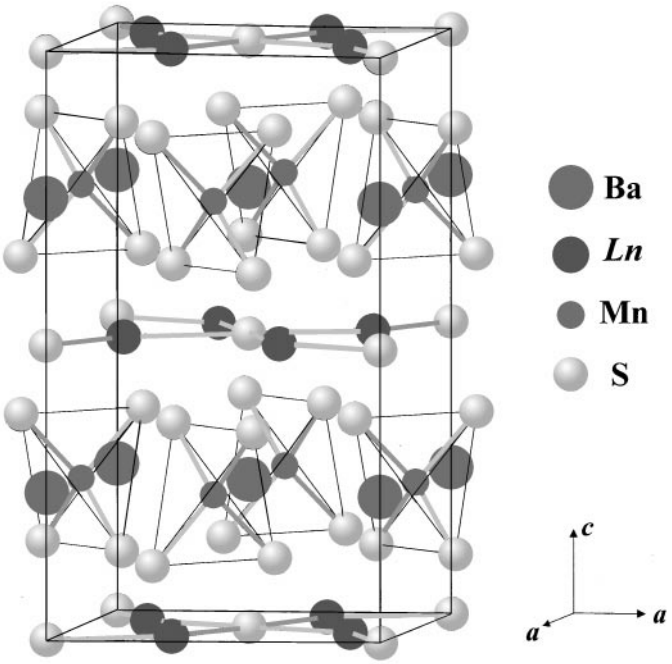

FIG. 1. Schematic structure of $BaLn_2MnS_5$ (Ln = La, Ce, and Pr).

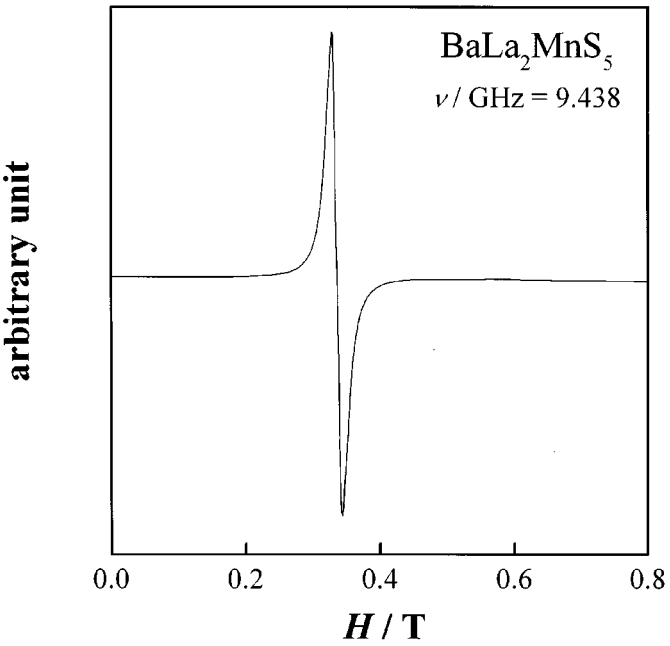

FIG. 3. EPR spectrum of Mn^{2+} in $BaLa_2MnS_5$ at room temperature.

a parameters. The obtained Mn–S(2) bond lengths (2.343 Å for $BaLa_2MnS_5$, 2.327 Å for $BaCe_2MnS_5$, and 2.338 Å for $BaPr_2MnS_5$) are shorter than the Mn–S length (2.500 Å) calculated from Shannon's ionic radius (8). Therefore, the Mn–S tetrahedra may be slightly compressed.

EPR Spectra

Figure 3 shows the EPR spectrum for $BaLa_2MnS_5$ in a magnetic field swept from 0 to 800 mT. The Mn ion is the only paramagnetic ion. A sharp single line is centered at 336.1 mT, and the g-value is calculated to be 2.00. This result shows that the Mn ion is in the divalent oxidations state and in the high spin state ($^6S_{5/2}$) with no orbital magnetic moment contribution. The EPR measurements of $BaCe_2MnS_5$ and $BaPr_2MnS_5$ showed spectra similar to that of $BaLa_2MnS_5$ and both of their g-values are also calculated to be 2.00. From these spectra, the Mn ions are found to be in divalent and high spin state ($^6S_{5/2}$) and the Ce and Pr ions are found to be in trivalent states in these compounds.

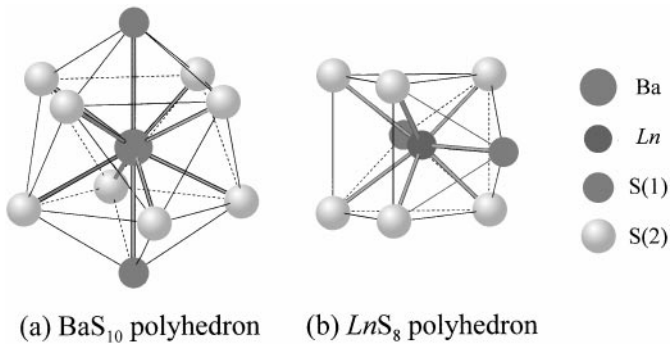

FIG. 2. Coordination of cations. (a) Sulfur ions around Ba ion. (b) Sulfur ions around Ln ion.

Magnetic Susceptibilities

Figure 4 shows magnetic susceptibilities as a function of temperature of $BaLa_2MnS_5$. This compound shows an antiferromagnetic behavior attributable to the magnetic ordering of the Mn^{2+} spins below 58.5 K. Figure 5 shows the magnetization at 1.8 K as a function of magnetic field. The absence of divergence between the ZFC and FC magnetic susceptibilities and no magnetic hysteresis in the magnetization vs magnetic field curve indicate that this compound transforms to a simple antiferromagnetic state without any weak ferromagnetic properties below 58.5 K. The magnetization is calculated to be 0.17 μ_B at 5 T and the higher magnetic field is required for saturating the magnetic moment of Mn^{2+} ($M_s = 5\ \mu_B$).

Figure 6 shows the temperature dependence of the ZFC magnetic susceptibilities of $BaCe_2MnS_5$ and $BaPr_2MnS_5$, indicating that both compounds show magnetic anomalies at 62 and 64.5 K, respectively. The differences in magnetic susceptibilities between the ZFC and FC are not observed

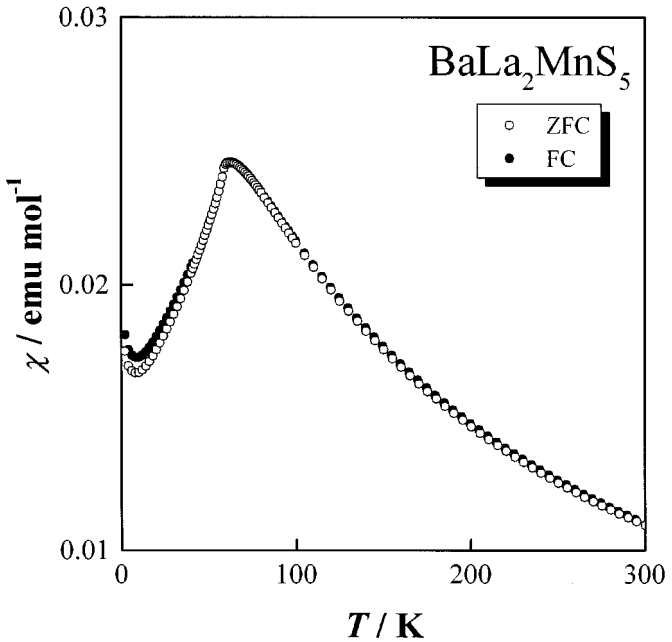

FIG. 4. Temperature dependence of the magnetic susceptibility of $BaLa_2MnS_5$.

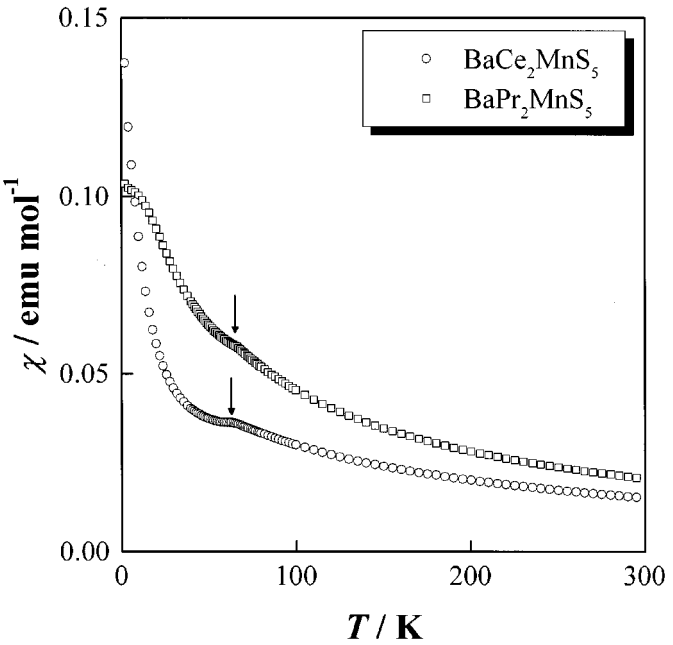

FIG. 6. Temperature dependence of the magnetic susceptibility of $BaCe_2MnS_5$ and $BaPr_2MnS_5$. Arrows show the magnetic transition temperatures (see text).

for both compounds. The curve of the magnetic susceptibility vs temperature for $BaPr_2MnS_5$ tends to flatten at temperatures below 20 K, while magnetic susceptibilities for $BaCe_2MnS_5$ increase markedly with decreasing temperature. In these compounds, the Mn^{2+} and Ln^{3+} (Ln = Ce and Pr) ions are both magnetic. These results suggest that below the magnetic transition temperatures the Mn^{2+} ions are in the antiferromagnetic ordered states and the Ln^{3+} ions are paramagnetic in $BaCe_2MnS_5$ and $BaPr_2MnS_5$. The Ln^{3+} ions are eight-coordinated and the crystal field symmetry is D_{2h}. The relatively low crystal field symmetry induces a singlet ground state for the Pr^{3+} ions (of which the electronic configuration is $[Xe]4f^2$). Therefore, the susceptibility for the $BaPr_2MnS_5$ become flattened at very low temperatures. On the other hand, since the Ce^{3+} ion has one unpaired electron, the susceptibility for the $BaCe_2MnS_5$ remarkably increases with decreasing temperature. The magnetic anomaly temperatures for $BaCe_2MnS_5$ and $BaPr_2MnS_5$ are almost the same as that for $BaLa_2MnS_5$, which indicates that the Ln^{3+} ions scarcely contribute to the antiferromagnetic superexchange interactions between the Mn^{2+} ions.

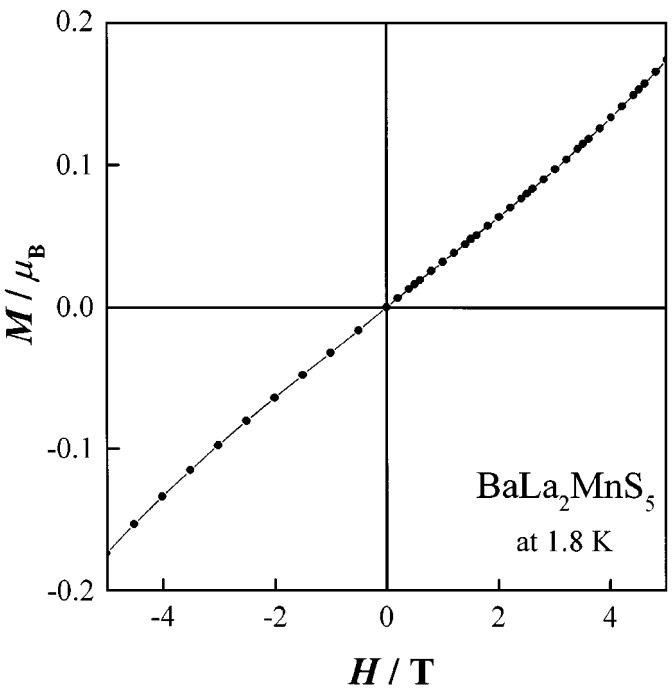

FIG. 5. Magnetic field dependence of the magnetization of $BaLa_2MnS_5$ at 1.8 K.

The temperature dependence of reciprocal magnetic susceptibilities of $BaLn_2MnS_5$ (Ln = La, Ce, and Pr) is shown in Fig. 7. The effective magnetic moment (μ_{eff}) and Weiss constant (θ) of $BaLa_2MnS_5$ are determined to be 5.94 μ_B and -96 K, respectively, applying the Curie–Weiss laws to the reciprocal susceptibility vs temperature curve in the high temperature region (150 K $\leq T \leq$ 300 K). This calculated moment (μ_{eff} = 5.94 μ_B) agrees well with the magnetic moment of the Mn^{2+} ion, which is in the $^6S_{5/2}$ state ($\mu_{eff} = g\sqrt{S(S+1)}\mu_B$ = 5.92 μ_B), and is consistent with the

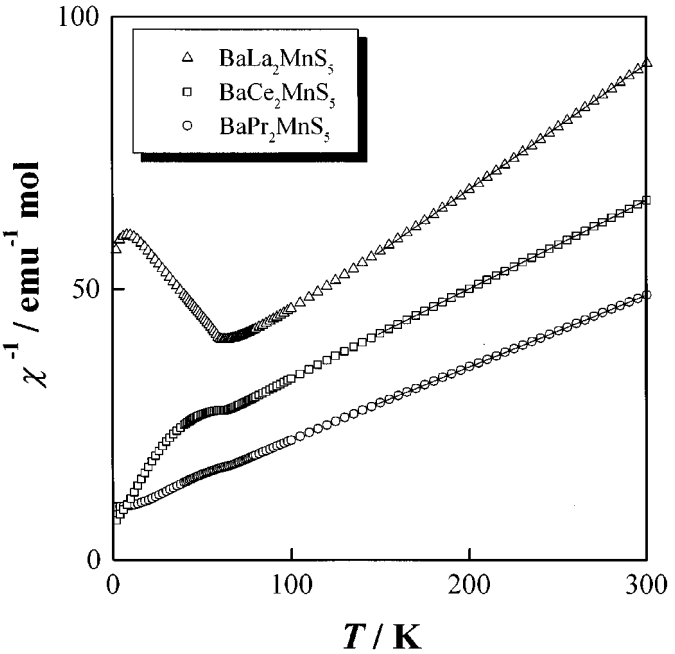

FIG. 7. Temperature dependence of the reciprocal magnetic susceptibility of BaLn_2MnS$_5$ (Ln = La, Ce, and Pr).

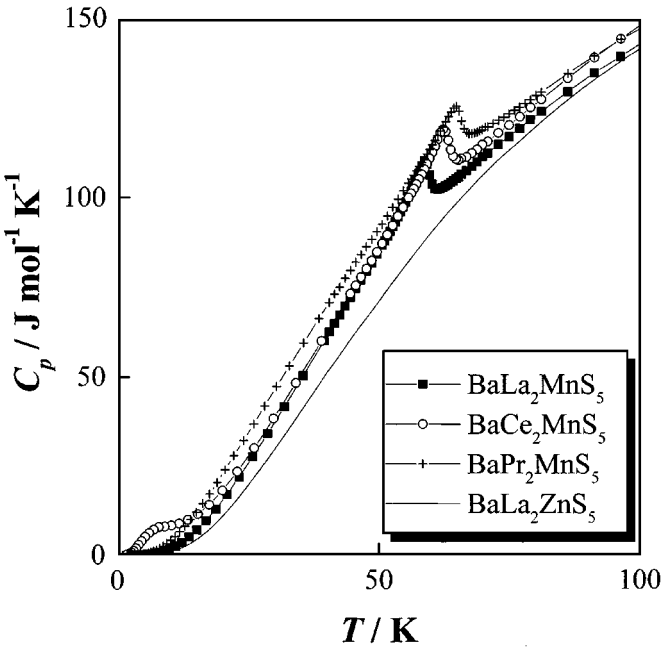

FIG. 8. Temperature dependence of the specific heat of BaLn_2MnS$_5$ (Ln = La, Ce, and Pr).

g-value obtained from the EPR measurement. Above 150 K, the effective magnetic moments of the Ce^{3+} and Pr^{3+} ion are calculated to be 2.58 and 3.50 μ_B, respectively, from the equation $\chi = N_A[\mu_{eff}(Mn^{2+})^2 + 2\mu_{eff}(Ln^{3+})^2]/3k_BT$ on the assumption that the moments of the Mn^{2+} ions in the $BaCe_2MnS_5$ and $BaPr_2MnS_5$ are both 5.94 μ_B. These values are in good agreement with the theoretical moments for the free Ce^{3+} and Pr^{3+} ions (2.54 μ_B for Ce^{3+} and 3.58 μ_B for Pr^{3+}). The values of μ_{eff} and θ determined for a series of BaLn_2MnS$_5$ are tabulated in Table 3.

Specific Heats

Figure 8 shows the variation of specific heat for BaLn_2MnS$_5$ (Ln = La, Ce, Pr) as a function of temperature. The λ-type anomalies have been observed at 58.5, 62, and 64.5 K for $BaLa_2MnS_5$, $BaCe_2MnS_5$, and $BaPr_2MnS_5$, respectively. These correspond to the magnetic anomalies found in their magnetic susceptibilities. In addition, the specific heat of $BaCe_2MnS_5$ shows another anomaly around 8 K.

The results of the specific heat measurements for $BaLa_2ZnS_5$ which has no paramagnetic ions are also shown in Fig. 8. If we assume that the electronic and lattice contributions to the specific heat are equal between $BaLa_2MnS_5$

TABLE 3
Magnetic Properties of BaLn_2MnS$_5$

	T_N/K	θ/K	$\mu_{eff}(Mn^{2+})/\mu_B$	$\mu_{eff}(Ln^{3+})/\mu_B$
$BaLa_2MnS_5$	58.5	−96	5.94	—
$BaCe_2MnS_5$	62	−105	(5.94)[a]	2.58
$BaPr_2MnS_5$	64.5	−67	(5.94)[a]	3.50

[a] Values in parentheses are the effective magnetic moments obtained from $BaLa_2MnS_5$.

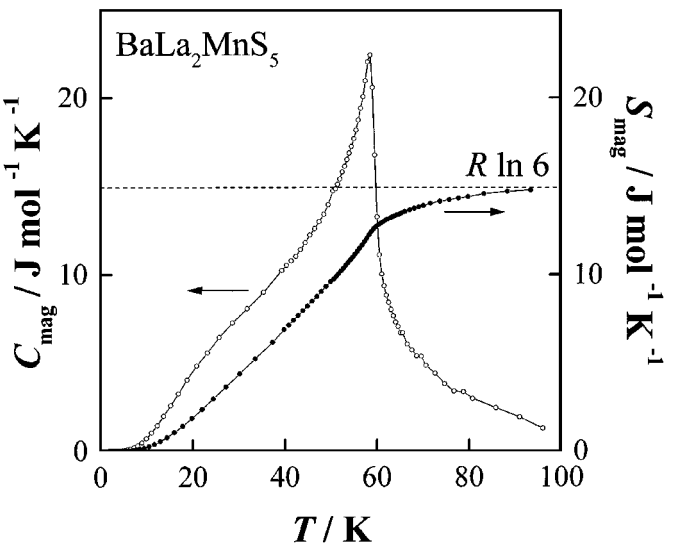

FIG. 9. Magnetic specific heat and magnetic entropy of $BaLa_2MnS_5$.

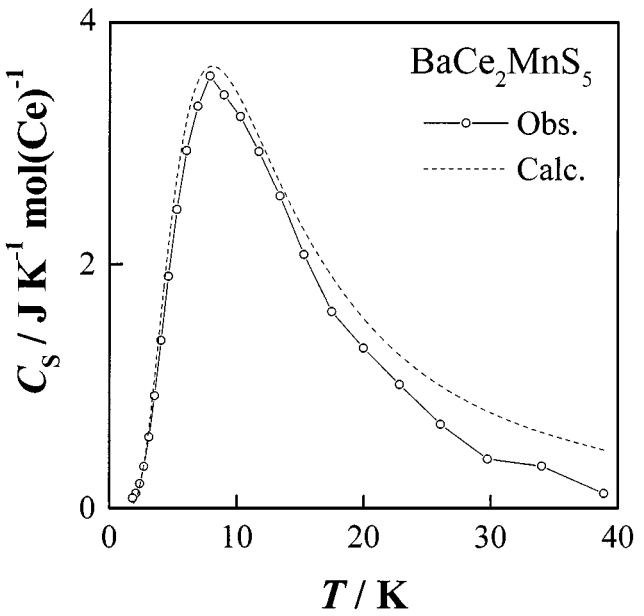

FIG. 10. Schottky-type specific heat of $BaCe_2MnS_5$, along with theoretical fit to the data (see text).

and $BaLa_2ZnS_5$, the magnetic specific heat for $BaLa_2MnS_5$ is obtained by subtracting the specific heat of $BaLa_2ZnS_5$ from that of $BaLa_2MnS_5$. Its temperature dependence is shown in Fig. 9. The magnetic entropy change associated with the Mn antiferromagnetic transition is calculated to be 14.76 J/mol K at 95 K, which is very close to

$$R\ln(2S+1) = R\ln\left(2\frac{5}{2}+1\right) = 14.90(\text{J/mol K}),$$

where R is a molar gas constant, and S is a total spin quantum number. This result indicates that the ground state for Mn^{2+} is $^6S_{5/2}$. Similar λ-type anomalies found for $BaCe_2MnS_5$ at 62 K and for $BaPr_2MnS_5$ at 64.5 K are also ascribable to the Mn antiferromagnetic transitions.

By subtracting the specific heat of $BaLa_2MnS_5$ from that of $BaCe_2MnS_5$, the residual specific heat which should be due to the properties of Ce^{3+} ion is obtained. Its temperature dependence is shown in Fig. 10. A Shottky-type anomaly has been found at 8 K. To discuss this anomaly, we consider the crystal field splitting of the $^2F_{5/2}$ state of the Ce^{3+} ion. We consider a level of degeneracy g_1 which is Δ in energy above a level of degeneracy g_0. For this two-level system, the Shottky specific heat is given by

$$C_s = \frac{R(\Delta/kT)^2(g_0/g_1)\exp(\Delta/kT)}{[1+(g_0/g_1)\exp(\Delta/kT)]^2}. \qquad [1]$$

The observed Schottky-type anomaly was fitted by using Eq. [1] as a broken line in Fig. 10. The energy separation (Δ) was estimated to be 19.2 K and the ratio g_0/g_1 was found to be one. The ground state of the Ce^{3+} ion should be a doublet under this low crystal field symmetry. Therefore, $g_0 = g_1 = 2$ and the ground state of the Ce^{3+} ion $^2F_{5/2}$ split into three Kramers' doublets.

REFERENCES

1. W. Bronger and P. Müller, *J. Alloys Compds.* **246,** 27 (1997).
2. I. E. Grey and H. Steinfink, *Inorg. Chem.* **10,** 691 (1971).
3. L. Guen, W. S. Glaunsinger, and A. Wold, *Mater. Res. Bull.* **14,** 463 (1979).
4. G. D. Albertelli, II, J. A. Cowen, C. N. Hoff, T. A. Kaplan, S. D. Mahanti, J. H. Liao, and M. G. Kanatzidis, *Phys. Rev. B* **55,** 11056 (1997).
5. T. Fries, Y. Shapira, F. Palacio, M. C. Morón, G. J. McIntyre, R. Kershaw, A. Wold, and E. J. McNiff, Jr., *Phys. Rev. B* **56,** 5424 (1997).
6. H. Masuda, T. Fujino, N. Sato, and K. Yamada, *J. Solid State Chem.* **146,** 336 (1999)
7. F. Izumi, *in* "The Rietveld Method" (R. A. Young, Ed.), Chap. 13. Oxford Univ. Press, Oxford, 1995.
8. R. D. Shannon, *Acta Crystallogr. A* **32,** 751 (1976).